4.2

Plasma Models

ANNEMIE BOGAERTS and RENAAT GIJBELS
University of Antwerp, Belgium

4.2.1 INTRODUCTION

To improve the analytical results of GDS techniques, a good insight into the GD source is desirable. One of the possible ways to achieve this is by mathematical modelling, i.e. a description of the behaviour of the plasma species by computer simulations. Three major approaches to the modelling of GDs can be found in the literature. The first one deals with the GD plasma as a fluid.[1–4] The species are assumed to be in hydrodynamic equilibrium and are described with continuity equations and flux equations based on diffusion and migration. This kind of model is only an approximation, especially for the fast electrons which are far from hydrodynamic equilibrium, since they gain more energy from the electric field than they lose by collisions. The second approach is a kinetic (Boltzmann) model[5,6] which copes with the non-equilibrium situation of the species by describing them with the Boltzmann transport equations. The third way is via Monte Carlo simulations.[7–9] The behaviour of the different species is simulated explicitly one after the other, based on Newton's laws for their trajectory and on random numbers for their collisions. By following a large number of particles (e.g. 10^5), statistically valid results can be obtained. This model is the most accurate one, because it deals with the particles on the lowest microscopic level. However, to reach satisfactory statistics, a longer calculation time is required than for the other two approaches. Hence, each model has its advantages and disadvantages. Therefore, it is desirable to use a combination of different models for different species in describing the GD. Species that are not in hydrodynamic equilibrium, like the electrons, must be treated with a Monte Carlo model, whereas species that are more or less in equilibrium, can be described with a fluid model.

Glow Discharge Optical Emission Spectrometry. Edited by R. Payling, D.G. Jones and A. Bengtson

We present here our modelling work for a direct current GD in argon. The models were developed for typical GD-MS discharge parameters (i.e. 1–10 mA, 500–1500 V, 50–150 Pa) but are also applicable, as shown later, for GD-OES conditions (higher currents and pressures). An overview and short description of the different models for the different species are given, and some typical results are shown.

4.2.2 OVERVIEW AND DESCRIPTION OF MODELS

The models presented here are one-dimensional, i.e. they apply to a discharge between two infinitely wide parallel plates so that the quantities vary only with distance from the electrodes. In the Monte Carlo simulations, however, three-dimensional motion of the species is already incorporated. The species that are assumed to be present in the plasma, include argon atoms at rest and uniformly distributed throughout the discharge (Ar^0), singly charged positive argon ions (Ar^+), fast argon atoms (Ar_f^0), argon metastable atoms (Ar_m^*), fast and slow electrons, and atoms and ions of the cathode material (M^0, M^+). Table 4.2.1 summarises the different models used to describe these species:

(a) **Fast electrons.** The fast electrons are simulated in the entire discharge by a Monte Carlo model. They start at the cathode and they are followed on their way through the discharge cell during successive timesteps. Their trajectory during the timestep Δt is calculated by Newton's laws:

$$z = z_0 + \nu_{z_0}\Delta t + \frac{e\mathrm{E}}{2m_e}(\Delta t)^2; x = x_0 + \nu_{x_0}\Delta t; y = y_0 + \nu_{y_0}\Delta t$$
$$\nu_z = \nu_{z_0} + \frac{e\mathrm{E}}{m_e}\Delta t; \nu_x = \nu_{x_0}; \nu_y = \nu_{y_0} \qquad (4.2.1)$$

where z_0, x_0, y_0 and z, x, y are the position co-ordinates before and after Δt; ν_{z_0},

Table 4.2.1 Overview of the different models used to describe the plasma species

Plasma species	Model
fast electrons	Monte Carlo (entire discharge)
slow electrons	fluid (entire discharge)
Ar^+ ions	fluid (entire discharge)
	Monte Carlo (CDS)
Ar_f^0 atoms	Monte Carlo (CDS)
Ar_m^* metastable atoms	fluid (entire discharge)
M^0 (thermalisation)	Monte Carlo (entire discharge)
M^0, M^+	
(diffusion, ionisation)	fluid (entire discharge)
M^+	Monte Carlo (CDS)

v_{x_0}, v_{y_0} and v_z, v_x, v_y are the velocities before and after Δt; E is the axial electric field; and e and m_e are the charge and mass of the electron.

The probability (Prob) of collision during the timestep Δt is calculated by:

$$\text{Prob} = 1 - \exp(-\Delta s \sum(n\sigma)) \tag{4.2.2}$$

where Δs is the distance travelled during Δt; n and σ are the densities of the target particles and the cross-sections of the different types of collision. This probability of collision is compared with a random number between 0 and 1. If the probability is lower than the random number, no collision occurs; if it is higher, there is a collision. The kind of collision that takes place and the new energy and direction after collision are also determined by random numbers. Collision processes incorporated in this model are total electron impact excit-

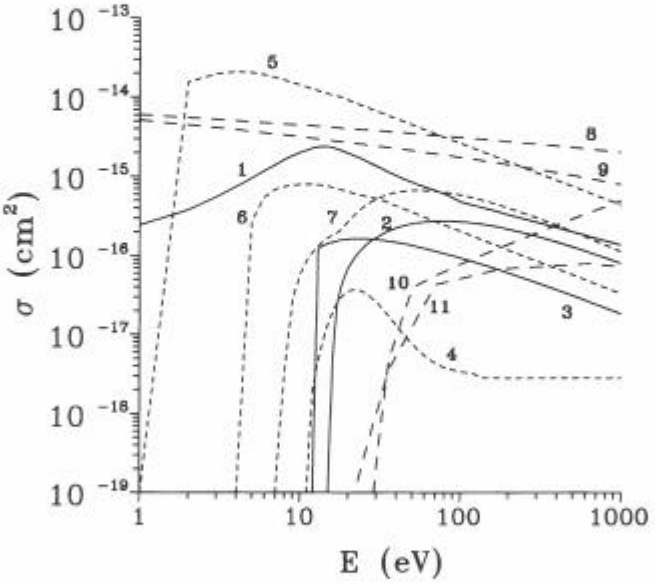

Figure 4.2.1. Cross-sections of the different collision processes of electrons, argon ions and fast argon atoms, incorporated in the models, as a function of the particle energies. 1: electron elastic collisions,[11,12] 2: electron impact ionisation of argon ground state atoms,[5] 3: total electron impact excitation from argon ground state atoms,[10] 4: electron impact excitation from argon ground state atoms to the metastable level,[13] 5: total electron impact excitation from the argon metastable levels,[14] 6: electron impact ionisation from the argon metastable levels,[15] 7: electron impact ionisation from the copper ground state atoms,[16] 8: symmetric charge transfer of the argon ions,[19] 9: elastic collisions of the argon ions and atoms,[8] 10: argon ion and atom impact ionisation, and argon atom impact excitation to the argon metastable levels,[20,21] 11: argon ion impact excitation to the metastable levels[21]

ation from the argon atom ground state and from the metastable level, electron impact ionisation of argon (from the ground state and from the metastable level) and of sputtered copper atoms (from the ground state), and elastic collisions. The cross-sections of these processes[5,10–16] are presented in Figure 4.2.1 (curves 1–7). The electrons formed within the plasma by ionisation collisions, are also treated in the same way. The electrons are followed from the position where they are formed until they collide with the walls or until they are showed down by collisions. Indeed, when their energies become lower than the excitation threshold of argon (ca 12 eV), they are transferred to the slow electron group (described in a fluid model, see further). A complete description of this model can be found in refs. 17 and 18.

(b) **Slow electrons and argon ions.** The behaviour of these species is described in the entire discharge with a fluid approach. The equations used are the continuity equations and flux equations based on diffusion and migration in the electric field, both for slow electrons and argon ions, together with the Poisson equation to obtain a self-consistent electric field (see equations (4.2.3–4.2.7)). Due to the severe non-linearity and the strong coupling of these five equations, solving this model is a difficult numerical problem. Details of the model and of the solution procedure can be found in ref. 18.

$$\frac{\partial n_i}{\partial t} + \frac{\partial J_i}{\partial x} = r_i \tag{4.2.3}$$

$$\frac{\partial n_e}{\partial t} + \frac{\partial J_e}{\partial x} = r_e \tag{4.2.4}$$

$$\frac{\partial^2 U}{\partial x^2} + \frac{e}{\epsilon_o}\left(n_i - n_e - n_{e(fast)}\right) = 0 \tag{4.2.5}$$

$$J_i = -\mu_i n_i \frac{\partial U}{\partial x} - D_i \frac{\partial n_i}{\partial x} \tag{4.2.6}$$

$$J_e = \mu_e n_e \frac{\partial U}{\partial x} - D_e \frac{\partial n_e}{\partial x} \tag{4.2.7}$$

where n, J, r, μ and D are the density, flux, creation rate, mobility and diffusion coefficient, respectively; subscripts i, e and *e(fast)* represent the argon ions, and the slow and fast electrons, respectively; U is the electric potential; and e and ϵ_0 are the elementary charge and the vacuum permittivity.

(c) Argon ions and fast argon atoms. Since the argon ions are not completely in hydrodynamic equilibrium in the cathode dark space (CDS) where a strong electric field is present, they are described in this region with a Monte Carlo model, together with the fast argon atoms that are created from the argon ions by symmetric charge transfer and by elastic collisions. The collision processes taken into account in this model, comprise symmetric charge transfer (only for the ions), elastic collisions, ion and atom impact ionisation and

excitation. The cross-sections of these processes[8,19–21] are shown in Figure 4.2.1 (curves 8–11). The model is described in more detail in refs. 17 and 22.

(d) Argon metastable atoms. These species are described in the entire discharge with a fluid model, consisting of a balance equation with all known production and loss processes (see equations (4.2.8 and 9)). The production processes include electron, argon ion and fast argon atom impact excitation, and argon ion-electron radiative recombination. The loss processes comprise electron impact ionisation and excitation from the metastable level, electron quenching to the nearby resonant levels, metastable–metastable collisions, Penning ionisation of sputtered atoms, two-body and three-body collisions with argon ground state atoms, and diffusion and subsequent de-excitation at the walls. A detailed description is found in ref. 23.

$$\frac{\partial n_{Ar_m^*}}{\partial t} - D_{Ar_m^*}\frac{\partial^2 n_{Ar_m^*}}{\partial x^2} = r_{prod}(x) - r_{loss}(x) \tag{4.2.8}$$

where

$$r_{prod}(x) = r_{e,exc}(x) + r_{i/a,exc}(x) + k_{recom}n_{e_s}(x)n_{Ar^+}(x) \tag{4.2.9}$$

$$r_{loss}(x) = r_{ion,met}(x) + r_{exc,met}(x) + k_{quen}n_{e_s}(x)n_{Ar_m^*}(x) + 2k_{met}[n_{Ar_m^*}(x)]^2 + k_{pi}n_M(x)n_{Ar_m^*}(x) + k_{2b}n_{Ar^0}n_{Ar_m^*}(x) + k_{3b}(n_{Ar^0})^2 n_{Ar_m^*}(x)$$

where r is the reaction rate of the various processes, k is the rate constant, and the other symbols are self-explanatory.

(e) Atoms and ions of the cathode material (Cu is taken as an example). When the atoms are sputtered from the cathode, they lose their initial energy of a few eV almost immediately by collisions with the gas particles. This so called thermalisation process is simulated with a Monte Carlo model, described in more detail in ref. 24. The further transport of the sputtered atoms is diffusion dominated. The transport of the sputtered atoms, their ionisation and the transport of the created ions (by diffusion and by migration in the electric field) are described with a fluid model in the entire discharge (see equations (4.2.10–15)). The ionisation processes considered in this model are Penning ionisation, asymmetric charge transfer and electron impact ionisation. Moreover, since the ions of the cathode material are not in hydrodynamic equilibrium in the CDS because of the high electric field, they are also treated, in this region, with a Monte Carlo model. Both models are described in detail in ref. 25.

$$\frac{\partial n_{Cu}(x)}{\partial t} + \frac{\partial J_{Cu}(x)}{\partial x} = r_{prod,Cu}(x) - r_{loss,Cu}(x) \tag{4.2.10}$$

$$\frac{\partial n_{Cu^+}(x)}{\partial t} + \frac{\partial J_{Cu^+}(x)}{\partial x} = r_{prod,Cu^+}(x) \tag{4.2.11}$$

$$J_{Cu}(x) = -D_{Cu}\frac{\partial n_{Cu}(x)}{\partial x} \tag{4.2.12}$$

$$J_{Cu^+}(x) = -D_{Cu^+}\frac{\partial n_{Cu^+}(x)}{\partial x} + \mu_{Cu^+} n_{Cu^+}(x)E(x) \tag{4.2.13}$$

$$r_{prod,Cu}(x) = J_0 F_T(x) \tag{4.2.14}$$

$$r_{loss,Cu}(x) = r_{prod,Cu^+}(x) = n_{Cu}(x)\,[r_{EI}(x) + k_{PI} n_{Ar^*_m}(x) + k_{CT} n_{Ar^+}(x)] \tag{4.2.15}$$

where J_0 is the flux of the sputtered atoms from the cathode; F_T is the thermalisation profile of the sputtered atoms, i.e. the distribution profile of positions at which the sputtered atoms are thermalised;[24] the remaining symbols have been explained before.

All the above models are coupled by the interaction processes among the plasma species. The combined models are solved iteratively until final convergence is reached, and provide an overall picture of the glow discharge.

4.2.3 RESULTS

Results are shown for a direct current GD in argon with a copper cathode, at a gas pressure of 500 Pa, a discharge voltage of 800 V and an electrical current of 40 mA, which are typical GD-OES discharge conditions. The gas temperature was set at 1000 K.[26] A theoretical discharge cell of 8 mm diameter and an effective anode backplate at 5 mm from the cathode was assumed. The models are only one-dimensional, although as mentioned for the Monte Carlo calculations the three-dimensional motion of the particles is already incorporated. Moreover, the cell is only a theoretical one, therefore the results obtained are still too early to be considered quantitative. Nevertheless, they do give a better insight into the GD.

4.2.3.1 DENSITIES OF THE PLASMA SPECIES

Figure 4.2.2 shows the densities of the different plasma species. The argon ion density (curve no. 1) is nearly constant in the CDS, increases rapidly in the beginning of the negative glow (NG) and reaches a maximum of about 2×10^{13} cm^{-3} halfway through the discharge, whereafter it decreases again. The slow electron density (curve no. 2) is almost zero in the CDS but is slightly higher than the argon ion density in the NG. It is nearly equal to the sum of the argon ion and copper ion densities in this region. This results in a net positive space charge in the CDS and nearly charge neutrality in the NG. The copper atom density (curve no. 3) is of the order of 4×10^{13} cm^{-3} at its maximum, close to the cathode, whereafter it decreases almost linearly towards the anode. The copper ion density (curve no. 4) has the same profile as the argon ion density and reaches a maximum of about 10^{12} cm^{-3}. Hence the copper ion to

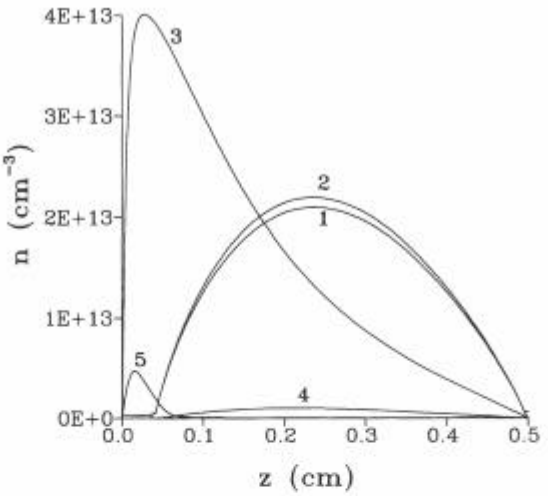

Figure 4.2.2. Density profiles of the plasma species, at 40 mA, 800 V, 500 Pa. (copper cathode in argon). 1: argon ions, 2: slow electrons, 3: sputtered copper atoms, 4: copper ions, 5: argon metastable atoms

argon ion density ratio is about 5%. When we compare this with the copper atom to argon atom density ratio of ca 10^{-4} (n_{Ar} is ca 3.6×10^{16} cm^{-3}), we conclude that the copper atoms are much more efficiently ionised than the argon atoms. This is also confirmed by comparing the calculated ionisation degrees of copper and of argon (the ionisation degree is the ion density to atom density ratio): the ionisation degree of copper was computed to be about 3.7% at these discharge conditions, whereas the calculated ionisation degree of argon is only about 0.05%.

The argon metastable atom density (curve no. 5) reaches a maximum relatively close to the cathode, which results from the different production and loss processes in equations (4.2.8 and 9). Indeed, beside electron impact excitation which is the most important production process in the NG, argon ion and atom impact excitation are also significant, especially close to the cathode;[23] this results in a maximum metastable density close to the cathode. Integrated over the total discharge, electron, ion and atom impact excitation are responsible for about 40%, 20% and 40% of the total argon metastable atom production, respectively. As noted, in the NG, the production is almost completely by electron impact excitation, whereas in the CDS it is almost entirely by ion and atom impact excitation.

The most important loss processes are electron quenching to the resonant levels (about 43% and dominant in the NG) and diffusion and de-excitation at

the walls (about 54% and dominant in the CDS). Metastable–metastable collisions, Penning ionisation of sputtered copper atoms, and electron impact excitation from the metastable levels are only of minor importance (each about 1%), and the other loss processes are almost negligible at these discharge conditions. The maximum metastable density is only of the order of 5×10^{12} cm^{-3}, which is clearly less than the argon ion and the copper atom densities. This is in contrast with typical GD-MS conditions (pressure of about 100 Pa) where these densities were calculated to be of the same order of magnitude.[23,27] It is indeed known from the literature that the argon metastable density does not increase greatly with pressure and can reach saturation at high pressures.[28,29]

The fast argon atom density (not shown) is about 10^{12} cm^{-3} in the CDS and zero in the NG. This is negligible compared to the overall argon atom density. Nevertheless the fast argon atoms play a non-negligible role in the GD, i.e. in cathode sputtering and in ionisation and excitation close to the cathode (see also further on). The fast electron density (not shown) is calculated to be of the order of 10^8 cm^{-3}, which is about five orders of magnitude lower than the argon ion and slow electron densities. Hence the fast electrons do not contribute to the space charge.

4.2.3.2 *ELECTRIC FIELD AND POTENTIAL DISTRIBUTIONS*

The potential and electric field distributions throughout the discharge are illustrated in Figure 4.2.3. The electric potential, which starts at −800 V at the

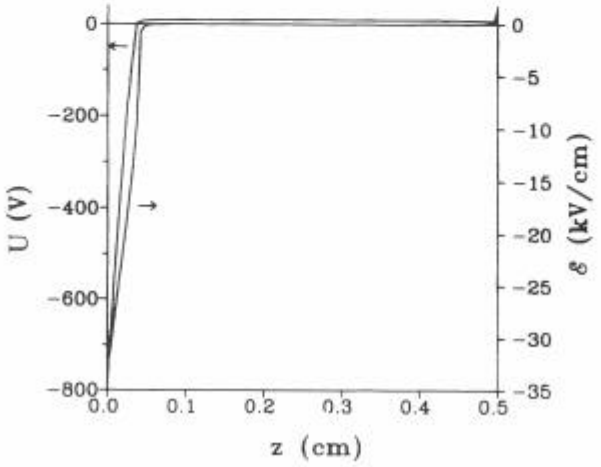

Figure 4.2.3. Electric field and potential distributions throughout the discharge, at 40 mA, 800 V, 500 Pa

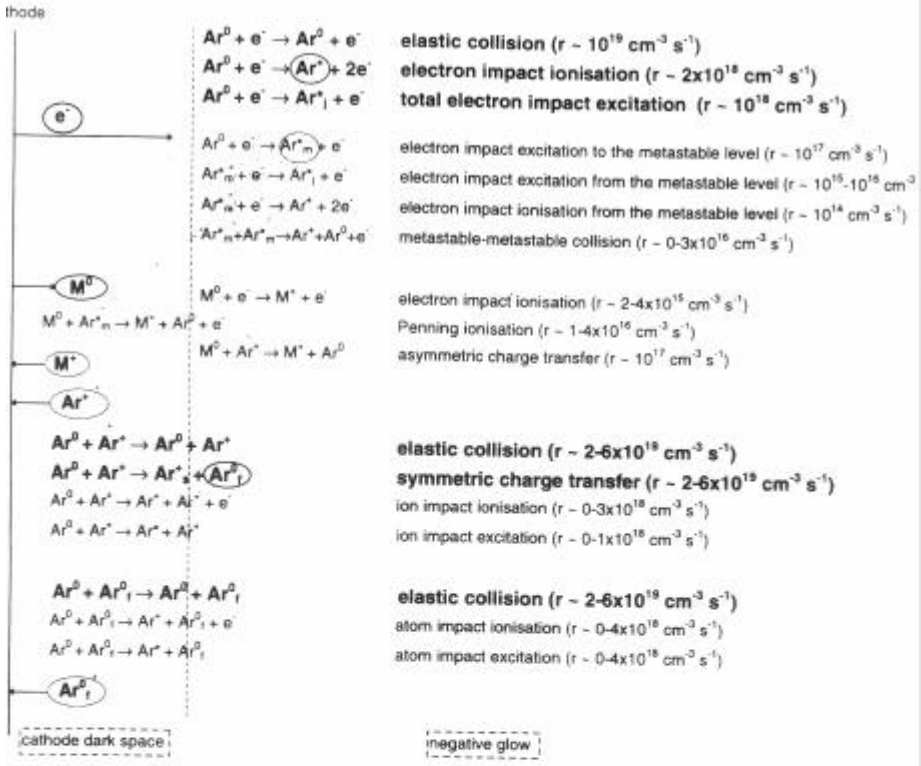

Figure 4.2.4. Schematic overview of the different collision processes in the glow discharge plasma, together with their collision rates calculated by the model, at 40 mA, 800 V, 500 Pa

cathode, shows a steep increase in the CDS and goes through zero at about 0.36 mm from the cathode. This position is defined as the interface between CDS and NG. The potential reaches a small positive value in the NG (ca. 8–10 V, which is called the plasma potential)) and returns to zero at the anode backplate. The electric field is very high at the cathode (about −32 kV/cm) and decreases rapidly in the CDS, it is small in the NG, changes sign nearly half-way through the discharge and increases to about 1750 V/cm at the anode backplate.

4.2.3.3 COLLISION RATES

The models also yield information about the occurrence of collision processes. Figure 4.2.4 presents an overview of the different collisions, together with their

collision rates (i.e. the number of collisions per cm^3 and per second), calculated by the model for the present discharge conditions (i.e. copper cathode, 40 mA, 800 V, 500 Pa). The Figure provides only information about the collision processes incorporated in the model. Other collisions can occur in the GD plasma, but were not included in the model, either because the relevant cross-section data could not be found in the literature (e.g. for the excitation of copper atoms) or because the collision processes are of low significance in the GD (e.g. collisions between two electrons, collisions between an electron and an ion, etc.).

The three major collision processes of the electrons are elastic collisions, electron impact ionisation and excitation of argon ground state atoms (presented in bold in the Figure). It can be seen that the excitation from the ground state to the metastable levels occurs at a rate one-tenth of the total excitation from the ground state. The excitation and ionisation from the metastable levels and the ionisation of the copper atoms are much less important, due to the lower densities of both the metastable atoms and the copper atoms. The collision processes of the argon ions and fast atoms take place only in the CDS. The most important collisions of the argon ions are symmetric charge transfer and elastic collisions. Also for the fast argon atoms, elastic collisions are the most significant (all presented in bold in the Figure). Argon ion and atom impact

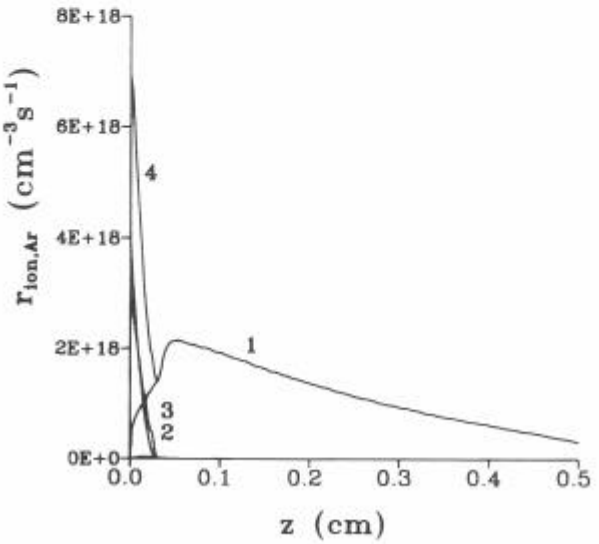

Figure 4.2.5. Relative contribution of different ionisation processes to the ionisation of argon, at 40 mA, 800 V, 500 Pa. 1: electron impact ionisation, 2: argon ion impact ionisation, 3: argon atom impact ionisation, 4: total ionisation of argon atoms

ionisation and excitation are only important close to the cathode, where the argon ions and atoms reach rather high energies.

Figure 4.2.5 shows the different ionisation rates of argon throughout the discharge. The major ionisation process is direct electron impact ionisation of ground state atoms (curve no. 1), although ion and atom impact ionisation become rather important in the CDS close to the cathode (curves nos. 2 and 3). The contribution of metastable–metastable collisions leading to the ionisation of one of the atoms is only small, and that of electron impact ionisation from the metastable levels is completely negligible at these discharge conditions. Integrated over the entire discharge, the relative contributions of the different processes amount to about 86.4% for electron impact, about 6.7% for ion and for atom impact, and about 0.2% for metastable–metastable collisions, and almost zero for electron impact ionisation from the metastable levels. Hence the argon metastable atoms are not significant for the formation of argon ions (i.e. two-step ionisation seems to be negligible at these discharge conditions). These relative contributions are slightly different in typical GD-MS conditions, where atom impact ionisation and metastable–metastable collisions are somewhat more important.[23]

Figure 4.2.6 illustrates the relative contribution of ionisation processes for the sputtered copper atoms. The cross-section of electron impact ionisation[16] was

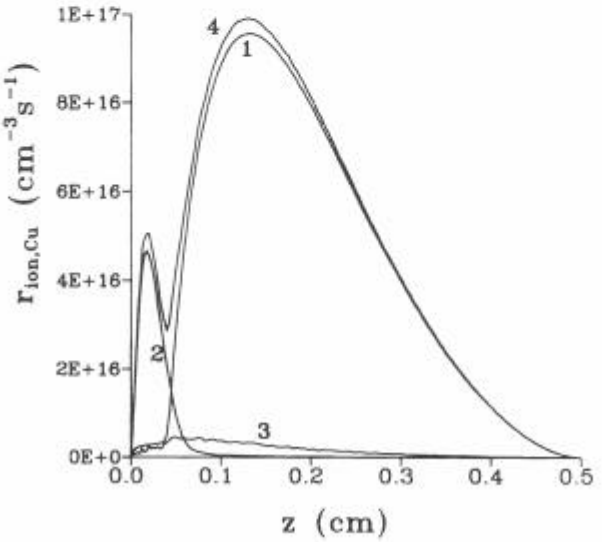

Figure 4.2.6. Relative contribution of different ionisation processes to the ionisation of copper, at 40 mA, 800 V, 500 Pa. 1: asymmetric charge transfer, 2: Penning ionisation, 3: electron impact ionisation, 4: total ionisation of copper atoms

presented in Figure 4.2.1. The rate constant of Penning ionisation could be obtained from an empirical formula,[30,31] i.e. $k_{PI} = 2.36 \times 10^{-10}$ cm^3 s^{-1}. The rate constant of asymmetric charge transfer is very difficult to find in the literature. The efficiency of this process depends on the availability of energy levels of the element ion which lie close to the argon ion ground or metastable levels. Literature data[32,33] show, however, that if the element ion possesses such energy levels, the rate constant of asymmetric charge transfer is comparable to the cross-section of Penning ionisation. Steers and Fielding have demonstrated the availability of suitable energy levels for asymmetric charge transfer between argon and copper,[34] therefore we assumed that the rate constants of asymmetric charge transfer and Penning ionisation are the same. It is seen in Figure 4.2.6 that asymmetric charge transfer (curve no. 1) is then the dominant ionisation process of the copper atoms at these discharge conditions. Penning ionisation (curve no. 2) seems only important in the CDS where the argon metastable atom density is at its maximum; electron impact ionisation (curve no. 3) is only of minor importance. Integrated over the total discharge, asymmetric charge transfer, Penning ionisation and electron impact ionisation contribute about 90%, 7% and 3%, respectively, to the total ionisation of copper atoms.

These data should, however, be considered with caution, due to the uncertainties in the rate constants. Nevertheless, even if the rate constant of asymmetric charge transfer is assumed to be much lower, this process remains the dominant ionisation process (e.g. for $k_{CT} = 5 \times 10^{-11}$ cm^3 s^{-1}, the relative contributions of asymmetric charge transfer, Penning ionisation and electron impact ionisation comprise about 63.3%, 27.3% and 9.3%). In typical GD-MS conditions, the relative contribution of Penning ionisation is more important or at least equally important (depending on the rate constant values) to asymmetric charge transfer. The statement that asymmetric charge transfer is the major ionisation process in GD-OES conditions (for elements which possess suitable ionic energy levels) and that Penning ionisation is dominant in typical GD-MS conditions is also found in the literature.[35] Our calculations predict that both in GD-MS[23] and GD-OES conditions, electron impact ionisation is only of minor importance for the ionisation of copper atoms. Due to the much more efficient Penning ionisation and/or asymmetric charge transfer, the copper atoms are much more efficiently ionised than the argon atoms, which was also demonstrated before (see Figure 4.2.2).

4.2.3.4 ENERGY DISTRIBUTIONS OF THE PLASMA SPECIES

The computer simulations can also give information about the energies of the different plasma species as a function of position in the cell. In Figure 4.2.7, the energy distribution of the electrons bombarding the anode backplate is presented. Most of the electrons have very low energies, but electrons of all energies are present in the plasma. Electrons can even reach the anode

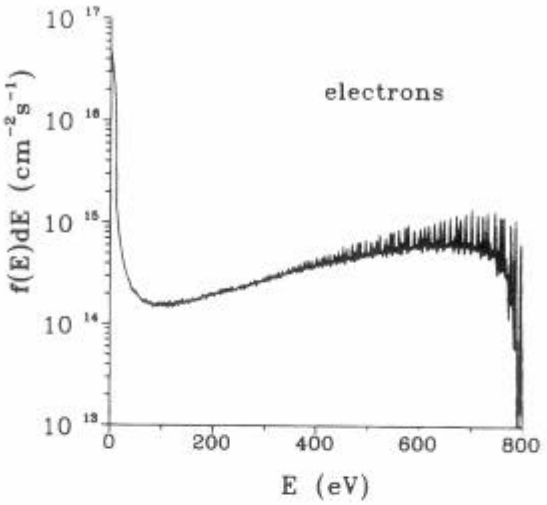

Figure 4.2.7. Energy distribution of the electrons bombarding the anode backplate, at 40 mA, 800 V, 500 Pa

backplate with the maximum energy, which means that they have not undergone inelastic collisions throughout the whole discharge. The low energy electrons are important in the GD to carry electrical current and to provide negative charge density. The fast electrons do not contribute significantly to the negative charge density. Their role exists primarily in causing inelastic collisions, thereby producing light emission (by excitation collisions) and the formation of new electrons and ions (by ionisation collisions) to sustain the discharge.

Figure 4.2.8 shows the energy distributions of the species bombarding the cathode plate. The energy distribution of the fast argon atoms is characterised by a rapidly decreasing curve towards higher energies. Also the argon ion energy distribution decreases towards higher energies. Indeed, the collision processes of the argon ions in the CDS (especially symmetric charge transfer and also elastic collisions) are efficient enough to give energy losses that can almost compensate for the energy gain from the electric field in this region. The energy of the fast atoms is still lower, since the atoms cannot gain energy from the electric field; they can only lose their energy by collisions. The decrease towards higher energies is, however, less pronounced than in typical GD-MS conditions.[17,25,27] Indeed, although the collision mean free path $\bar{l}_i$ of the ions is lower for typical GD-OES conditions than for GD-MS (i.e. for 500 Pa, 1000 K: $\bar{l}_i$ is about 0.06 mm, whereas for 100 Pa, 300 K: $\bar{l}_i$ is about 0.09 mm), the CDS is much thinner for GD-OES than for GD-MS (i.e. about 0.36 mm at 500 Pa, 1000 K, compared to about 1.5 mm at 100 Pa, 300 K[22]): therefore the total

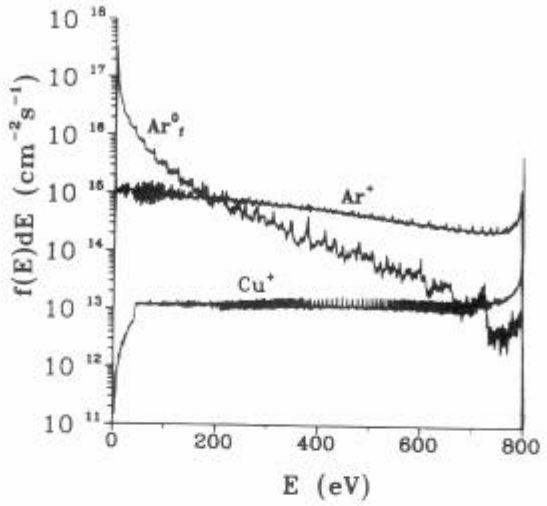

Figure 4.2.8. Energy distribution of the argon ions (Ar^+), fast argon atoms (Ar_f^0) and copper ions (Cu^-) bombarding the copper cathode, at 40 mA, 800 V, 500 Pa

number of collisions of the argon ions in the CDS is smaller for GD-OES than for GD-MS by a factor of 2.8. Hence, since the ions will not lose so much energy by collisions on their way through the CDS in GD-OES conditions, they will bombard the cathode with relatively higher energies. A small peak is even observed at maximum energy, which represents the argon ions that have traversed the entire CDS without collisions. Nevertheless, most of the argon ions have low energies.

Unlike the energy distributions of the argon ions and fast argon atoms, the energy distribution of the copper ions at the cathode is characterised by a pronounced peak at maximum energy. Indeed, the copper ions will not lose as much energy in the CDS as the argon ions, since they undergo only elastic collisions and almost no charge transfer collisions (i.e. asymmetric charge transfer of copper ions with argon atoms has a lower cross-section and symmetric charge transfer with copper atoms is also of low importance due to the low copper atom density compared to argon atom density). Both the energy distributions of the argon ions and copper ions bombarding the cathode at typical GD-MS conditions were in satisfactory agreement with experimental measurements on the VG 9000 GD mass spectrometer.[36] Since the efficiency of sputtering increases with the energy of the bombarding particles in the energy range considered here,[37] it is expected that the contribution of the copper ions to the sputtering process (self-sputtering) is non-negligible, in spite of their lower flux compared to the argon ion and fast argon atom fluxes. The relative

contributions to sputtering of the different bombarding species were calculated to be about 63%, 33% and 4%, for the argon ions, fast argon atoms and copper ions, respectively. This is slightly different from the typical GD-MS results, where the fast argon atoms yield the major contribution (i.e. typically 50–80%);[25] the reason is that the argon ions will undergo fewer collisions in the shorter CDS at GD-OES conditions, thereby creating fewer fast argon atoms than in the GD-MS situation. It should be noted that, although the argon ions and fast argon atoms account for the majority of sputtering, the role of copper ions (self-sputtering) cannot be neglected.

4.2.4 SUMMARY

A combination of different mathematical models for different plasma species is presented to give an overall description of the direct current GD in argon. Some typical results of the models are illustrated, like the density profiles of the plasma species, the electric field and potential distribution throughout the discharge, the different ionisation mechanisms in the plasma, the energy distributions of the different plasma species and relative contribution to sputtering. More details and more results (albeit for typical GD-MS conditions) can be found in the cited papers.

Moreover, the models are in principle also able to predict other quantities of interest to GD-OES users, like the excitation to different levels and hence the (relative) intensities of different spectral lines, but it is necessary to have cross-section data for the computer simulations. Unfortunately, these are not always easily found in the literature.

Since the present models apply only to a 'theoretical' one-dimensional cell, they provide a qualitative picture of the GD rather than quantitative results. In the future, the models will be extended to three dimensions and applied to more realistic cell geometries. To check the validity of the models, they will have to be controlled by plasma diagnostic measurements. Nevertheless, at this stage, the models can already provide better insight into the GD.

REFERENCES

[1] J.P. Boeuf, *Phys. Rev. A* **36**, 2782 (1987).
[2] J.P. Boeuf, *J. Appl. Phys.* **63**, 1342 (1988).
[3] J.D.P. Passchier and W.J. Goedheer, *J. Appl. Phys.* **73**, 1073 (1993).
[4] J.D.P. Passchier and W.J. Goedheer, *J. Appl. Phys.* **74**, 3744 (1993).
[5] R.J. Carman, *J. Phys. D* **22**, 55 (1989).
[6] I. Abril, *Computer Physics Comm.* **51**, 413 (1988).
[7] J.P. Boeuf and E. Marode, *J. Phys. D* **15**, 2169 (1982).
[8] Z. Wronski, *Vacuum* **42**, 635 (1991).

[9] J. Sun, Ye Gong and D. Wang, *J. Phys. D* **26**, 436 (1993).
[10] E. Eggarter, *J. Chem. Phys.* **62**, 833 (1975).
[11] W.C. Fon, K.A. Berrington, P.G. Burke and A. Hibbert, *J. Phys. B*, **16**, 307 (1983).
[12] F.J. de Heer, R.H.J. Jansen and W.J. van der Kaay, *J. Phys. B*, **12**, 979 (1979).
[13] N.J. Mason and W.R. Newell, *J. Phys. B* **20**, 1357 (1987).
[14] H.A. Hyman, *Phys. Rev. A* **18**, 441 (1978).
[15] H.A. Hyman, *Phys. Rev. A* **20**, 855 (1979).
[16] L. Vriens, *Phys. Lett.* **8**, 260 (1964).
[17] A. Bogaerts, M. van Straaten and R. Gijbels, *Spectrochim. Acta* **50B**, 179 (1995).
[18] A. Bogaerts, R. Gijbels and W.J. Goedheer, *J. Appl. Phys.* **78**, 2233 (!995).
[19] R.S. Robinson, *J. Vac. Sci. Technol.* **16**, 185 (1979).
[20] P.O. Haugsjaa and R.C. Amme, *J. Chem. Phys.* **52**, 4874 (1970).
[21] A.V. Phelps and B.M. Jelenkovic, *Phys. Rev. A* **38**, 2975 (1988).
[22] A. Bogaerts and R. Gijbels, *J. Appl. Phys.* **78**, 2233 (1995).
[23] A. Bogaerts and R. Gijbels, *Phys. Rev. A* **52**, 3743(1995).
[24] A. Bogaerts, M. van Straaten and R. Gijbels, *J. Appl. Phys.* **77**, 1868 (1995).
[25] A. Bogaerts and R. Gijbels, *J. Appl. Phys.* **79**, 1279 (1966).
[26] N.P. Ferreira, H.G.C. Human and L.R.P. Butler, *Spectrochim. Acta* **35B**, 287 (1980).
[27] A. Bogaerts and R. Gijbels, *Fres. J. Anal. Chem.* **355**, 853 (1996).
[28] R.L. Smith, D. Serxner and K.R. Hess, *Anal. Chem.* **61**, 1103 (1989).
[29] K.A. Hardy and J.W. Sheldon, *J. Appl. Phys.* **53**, 8532 (1982).
[30] L.A. Riseberg, W.F. Parks and L.D. Schearer, *Phys. Rev. A* **8**, 1962 (1973).
[31] S. Inaba, T. Goto and S. Hattori, *J. Phys. Soc. Jpn.* **52**, 1164 (1983).
[32] P. Baltayan, J.C. Pebay-Peyroula and N. Sadeghi, *J. Phys. B.* **18**, 3615 (1985).
[33] P. Baltayan, J.C. Pebay-Peyroula and N. Sadeghi, *J. Phys. B.* **19**, 2695 (1986).
[34] E.B.M. Steers and R.J. Fielding, *J. Anal. Atom. Spectrom.* **2**, 239 (1987).
[35] M.K. Levy, D. Serxner, A.D. Angstadt, R.L. Smith and K.R. Hess, *Spectrochim. Acta* **46B**, 253 (1991).
[36] M. van Straaten, A. Bogaerts and R. Gijbels, *Spectrochim. Acta* **50B**, 583 (1995).
[37] N. Matsunami, Y. Yamamura, Y. Itikawa, N. Itoh, Y. Kazumata, S. Miyagawa, K. Morita, R. Shimizu and H. Tawara, *Atom. Data Nucl. Data Tables* **31**, 1 (1984).